Characterization of a [4Fe-4S]-Ferredoxin Model Based on a Concave Tetradentate Thiol Ligand System

Constantinus F. Martens[a], Mathias M. G. Bongers[a], Paul J. A. Kenis[a], Ryszard Czajka[b], Martinus C. Feiters*[a], Johannes G. M. van der Linden[c], and Roland J. M. Nolte[a]

Department of Organic Chemistry, Nijmegen SON Research Centre[a],
Department of Experimental Solid State Physics[b],
Department of Inorganic Chemistry[c],
University of Nijmegen, Toernooiveld, NL-6525 Nijmegen, The Netherlands

Received March 19, 1996

Keywords: Cavitand / Electrochemistry / Iron sulfur cluster / Metalloprotein model

NMR and Mössbauer spectroscopy show that a novel tetrathiol ligand, based on the cavitand diphenylglycoluril, encapsulates a 4Fe-4S cluster and induces asymmetry in it. The cluster gives a weak electrochemical current response in DMF, with a half-wave potential for the $2^-/3^-$ reduction vs. Fc^+/Fc of -1.7 V. Ba^{2+} ions are adsorbed, according to X-ray analysis of the SEM image of the electrode, and act as modulator and promoter of the electrochemical response. On the basis of cyclic voltammograms it is proposed that this adsorption creates electroactive sites, changing the type of diffusion controlling the mass transport to the electrode from radial to linear, and that it helps the negatively charged complex, which contains a dipole, to approach the negative electrode in an orientation favourable for electron exchange. This feature makes the complex an important model for ferredoxins, in spite of a difference in redox potential.

Introduction

Iron is the most widely distributed transition metal in biology. Besides playing an important role in numerous catalytic transformations[1], the main tasks it fulfils are those of electron transfer[2] and dioxygen transport[3], the latter as heme iron in myoglobin[4] and hemoglobin[5], and as nonheme iron in hemerythrin[6]. The iron proteins responsible for electron transport are the cytochromes and a variety of iron-sulfur proteins, including the so-called 4-iron 4-sulfur proteins[7]. These 4Fe-4S proteins are involved in a variety of biological redox processes, viz. photosynthesis[8,9] nitrogen fixation[10] and respiration[11]. Two classes of 4Fe-4S proteins can be distinguished: the ferredoxins (Fd), whose core oxidation states shuttle between 2^+ and 1^+ at potentials ranging from -250 to -650 mV in water vs. NHE, and the so-called high-potential iron-sulfur proteins (HiPIP) whose cores cycle between 3^+ and 2^+ oxidation states at potentials ranging from $+50$ to $+450$ mV vs. NHE.

Since no major differences are noted between the cores of Fd's and HP's, other factors must be responsible for the "fine-tuning" of the redox behaviour. Most likely these factors are H-bonding[12,13], accessibility of the core for solvent molecules[12], type of solvent molecule[14], hydrophobicity of the protein shell[14], and (in model systems) the nature of the thiolate ligand coordinating to the core. In model systems it is possible to vary conditions and ligands in a relatively simple way and thus to influence the redox behaviour of the [4Fe-4S] cluster. These models may mimic certain aspects of metalloproteins, thereby helping to understand the complex reaction behaviour of these biomolecules. Eventually, the model approach is expected to lead to new insights and also to assist in the rational design of catalysts.

Current efforts in the design of iron-sulfur protein analogues focus on the use of cavitands and other macrocyclic ligand systems to coordinate the [4Fe-4S] core. Recent examples include modified cyclodextrins[15], macrocycles[16,17], cavitands based on hexa-substituted benzenes[18,19], and cyclotriveratrylene[20]. A variety of goals are being pursued, including the improvement of the aqueous solubility of the formed cluster, the creation of a specific iron subsite, and the mimicking of the hydrophobic HP protein pocket by encapsulation of the 4Fe-4S cluster. In recent years, we have explored the chemistry of cavitands based on diphenylglycoluril, yielding clips[21] and baskets[22] that selectively bind dihydroxybenzenes. Such baskets have been extended with ligand sets for rhodium[23] and copper[24] ions to yield selective catalysts. In this paper we describe the detailed characterization of a diphenylglycoluril-based concave tetra-thiol ligand system **3**, capable of coordinating a [4Fe-4S] cluster[25]. The [4Fe-4S] core in the cluster complex **4** is semi-encapsulated and exhibits an electrochemical behaviour similar to that described for metalloproteins[26], apart from a large difference in redox potential.

Results and Discussion

Ligand Synthesis

The tetrathiol ligand **3** was synthesized as shown in Scheme 1. The starting compound **1** was prepared by a previously published five-step synthetic route[27]. Treatment of **1** with cesium thioacetate[28] gave the fully protected tetrathiol **2**. The X-ray structure of **2** is presented in Figure 1. Details of the structure elucidation have been given elsewhere[25]. As can be seen from this figure the overall shape

  0009–2940/97/0101–0023 $ 15.00+.25/0

of the ligand is concave. Its convex side is shielded by two phenyl rings. The central part is a cavity whose bottom is lined by two fused 2-imidazolidone rings. The walls of the cavity are formed by two diverging *o*-xylylene rings. At the base of the cavity, where these rings are attached to the imidazolidone framework, their spacing is approximately 5.7 Å. The centres of the rings are 6.62 Å apart, and at the top their separation is 7.5 Å. The oxygen atoms of the carbonyl groups are 5.55 Å apart. The angle of the imidazolidone C=O group with the axis through the carbonyl carbon atoms is 38.7°. Previous NMR studies have proved that the cavity is rigid and stays intact in the temperature range from −95 to 150 °C[21]. The cavity is large enough (>100 Å^3) to accomodate an $[Fe_4S_4]^{2+}$ cluster (volume 87.6 Å^3)[29].

Scheme 1

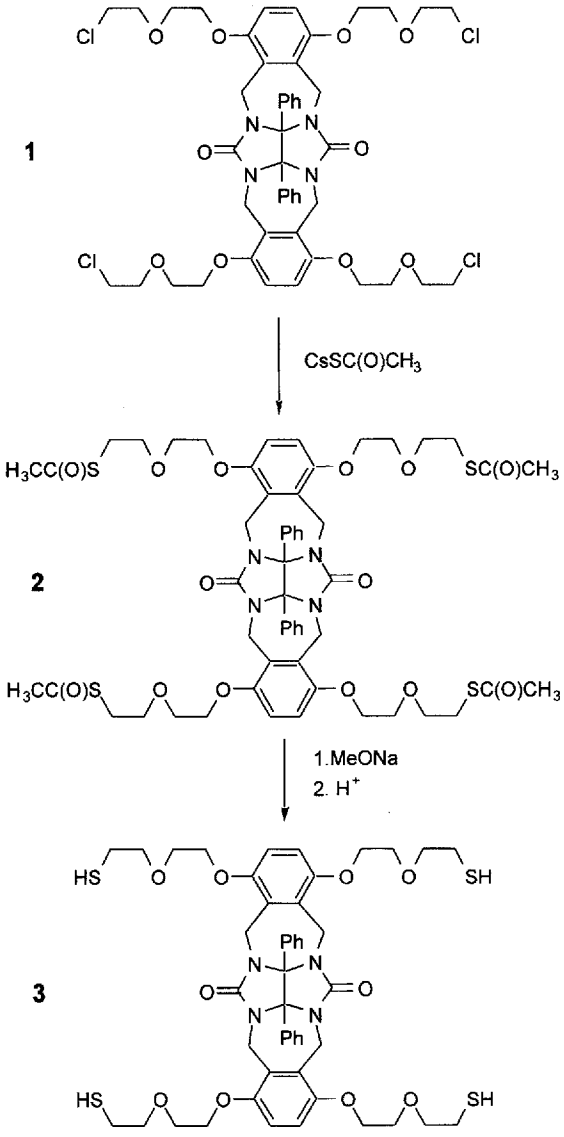

The protecting groups in **2** where cleaved off quantitatively using sodium methoxide followed by acidic work-up, or by reaction with $LiAlH_4$. Both procedures yielded a fully deprotected ligand (90% after work-up). In the IR spectra

Figure 1. X-ray structure of **2**

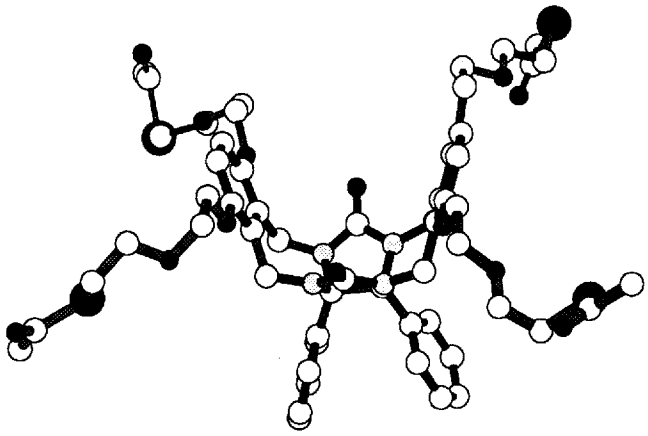

of **3** the presence of the thiol groups was confirmed by an absorption band at ca. 2542 cm^{-1}[30]. The ^{1}H-NMR spectrum of **3** in $CDCl_3$ showed a triplet for the SH groups at δ = 1.62 with the correct integration.

Incorporation of the Fe_4S_4 Cluster into the Ligand

Usually exchange reactions or incorporation of iron-sulfur clusters into thiol ligand sets are accomplished with $[Fe_4S_4(SR)_4]^{2-}$ (R = Et or *t*-Bu) as the starting clusters[31]. The more acidic thiol of the new ligand displaces the thiolate from the cluster core[32]. In our case the difference in pK_a between the thiol in the ligand and the thiol in the starting cluster is not large. Even though the liberated thiols are usually volatile and are removed from the reaction mixture by applying a dynamic vacuum, this feature may complicate the exchange reaction and cause the formation of mixed cluster species. In order to prevent these side reactions we chose to use $[Fe_4S_4Cl_4]^{2-}$ as the starting cluster[33]. The labile chloride ions in this cluster were readily displaced from the core by the thiolate groups[34], generated in situ from **3** with $(n\text{-Bu})_4NOH$ in dimethylformamide (DMF). In an alternative procedure we directly added the tetra sodium salt of **3** to the cluster. During the reactions, a colour change from purple-black to brownish-black was observed. Both procedures gave the cluster complex **4** in good yields (70−80%). The products obtained from both reactions were identical and pure according to ^{1}H NMR and electrochemistry. Complex **4** is only soluble in polar solvents such as DMF or dimethylsulfoxide (DMSO). It was purified by precipitation with diethyl ether and subsequent washing of the precipitate with acetonitrile. Redissolving **4** in DMF and slow diffusion of diethyl ether into this solution yielded the complex as long, black needles. Unfortunately, these needles were not suitable for X-ray diffraction. The UV-Vis spectrum of **4** in DMF is very similar to that of the related $Fe_4S_4(SEt)_4^{2-}$ cluster. The latter shows absorption bands at 297 and 418 nm (ε = 23300 and 17200 l mol^{-1} cm^{-1}, respectively). The spectrum of **4** is slightly blue shifted and has comparable extinction coefficients: λ_{max} = 295 and 412 nm (ε = 25500 and 13100 l mol^{-1} cm^{-1}, respectively).

NMR

The ^{1}H-NMR spectrum of a solution of **4** in [D$_6$]DMSO at 353 K (Figure 3a) showed two different sets of signals for the methylene protons next to the coordinating sulfur atoms, viz. at δ = 14.08 and 15.11. These signals displayed the expected[35] paramagnetic broadening and shift for protons adjacent to a [4Fe-4S] core. No coalescence of the methylene protons is observed in the temperature range 300–370 K. The approximate values for the integration of the δ = 14.08 and δ = 15.11 signals are 6.0 and 0.6 protons, respectively, but the fact that these values do not add up to the required 8 protons indicates that they are not reliable, probably because of the enhanced relaxation due to the paramagnetism. The occurrence of two sets of such protons is consistent with our proposal that the core is tilted and pointing towards the cavity, as indicated schematically in Figure 2(a). CPK models show that the cluster core and ligand match very well [see Figure 2(b) and (c)]. The incorporation yields an asymmetric compound, because unlike the free ligand **3**, the cluster complex no longer has C_2 symmetry. One of the arms of the ligand has to approach the cluster from the bottom of the cavity in order to be able to coordinate to the core, while another arm has to coordinate from the top. This yields a complex in which the aromatic protons of the xylylene-walls flanking the cavity become inequivalent. In accordance with this, the singlet signal originally observed for these protons was found to be split. The cavity in the cluster complex is probably quite distorted as the doublets for the NCH$_2$Ar protons in **4** were broadened and formed one singlet at δ = 5.5. This signal showed a small temperature dependence and sharpened upon increasing the temperature. Evidence for incorporation of the [4Fe-4S] cluster into ligand **3** also comes from the ^{13}C-NMR spectrum, recorded at 308 K (Figure 3b). The signals of the CH$_2$S-carbon atoms were considerably broadened and had shifted by ca. δ = 70 downfield from their original position to δ = 102. The position and the magnitude of the isotropic shift are in accordance with values previously reported for [Fe$_4$S$_4$[(SEt)$_4$]$^{2+}$ and related complexes[36,37]. The proposed asymmetry of the complex is confirmed by the appearance of double signals for the carbon atoms in the xylene walls of the cavity and in the spacer arms.

Evidence for the presence of an intact cluster core comes from the following experiments. First, measurements of the temperature dependence of the isotropic shifts show that the two sets of CH$_2$S protons shift by δ = 1.7 downfield if the temperature is increased over a range of 70 degrees (Figure 3c). This value for the shifts, which is explained by an increase in population of the excited low-lying paramagnetic state relative to that of the diamagnetic ground state, corresponds with those reported in the literature[35]. Secondly, the addition of an excess of PhSH to **4** results in the extrusion of the [4Fe-4S] core from **4** and the formation of the known cluster complex [Fe$_4$S$_4$(SPh)$_4$]$^{2-}$. The chemical shift values found for the latter derivative in [D$_6$]DMSO are δ = 5.50 (*p*-PhH), 5.80 (*o*-PhH) and 8.20 (*m*-PhH); reported values ([D$_3$]CH$_3$CN) are δ = 5.28, 5.88 and 8.18, respectively[35].

Figure 2. Schematic drawing of complex **4** (a); space-filling models of **4**: side view (b) and top view (c)

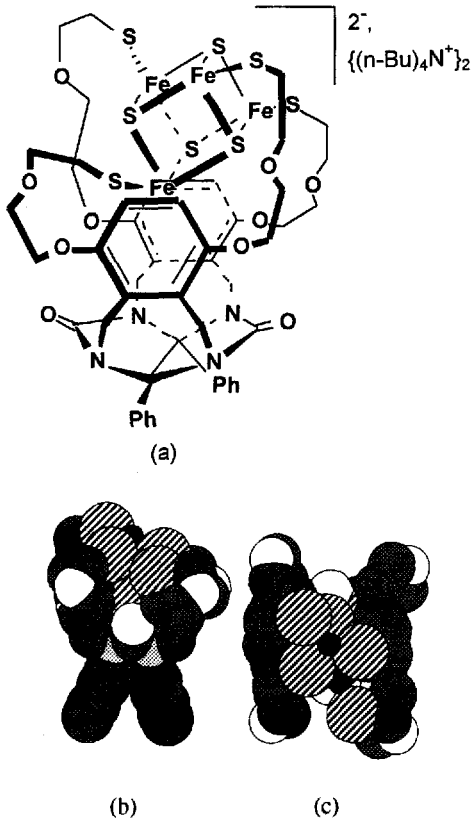

Mössbauer Spectroscopy

The presence of an intact [4Fe-4S] core in **4** was also checked with Mössbauer spectroscopy. The ^{57}Fe Mössbauer spectra of model compounds as well as ferredoxins exhibit a simple quadrupole doublet with an isomer shift of approximately 0.40 mm s^{-1}[38]. The room temperature spectrum of **4** (Figure 4a) shows a doublet typical of a [4Fe-4S] core. When the temperature is lowered to 77 K (Figure 4b) the spectrum shows the normal broadening but no additional information is obtained. The values obtained for both the isomer shift and the quadrupole splitting in the low-temperature measurement (0.48 and 1.42 mm s^{-1}, respectively) are slightly different from the values measured at room temperature (respectively 0.55 and 1.30 mm s^{-1}). Upon comparison with the spectrum of the starting cluster [Fe$_4$S$_4$Cl$_4$]$^{2-}$ (Figure 4c) the line broadening in **4** is evident; whilst the spectrum of [Fe$_4$S$_4$Cl$_4$]$^{2-}$ can be fitted with the natural line width for ^{57}Fe, this is not possible for **4**. A possible explanation might be that the relaxation processes operative in **4** are slightly different from those in [Fe$_4$S$_4$Cl$_4$]$^{2-}$. However, if this were the case, lowering of the temperature should have had a more distinct effect. It is likely that the slightly different electronic environments around each iron atom in **4**, which are caused by the asymmetric encapsulation by the cavitand, lead to line broadening in the Mössbauer spectrum. The fact that different electronic environments influence the positions of the lines in the spectrum is also indicated by the fact that the quadrupole split-

Figure 3. (a) and (b) 400-MHz ^{1}H- and ^{13}C-NMR spectra, respectively, of **4** in DMSO; (c) temperature dependence of the isotropic shift of each of the CH_2S protons in **4** (solvent $[D_6]$DMSO)

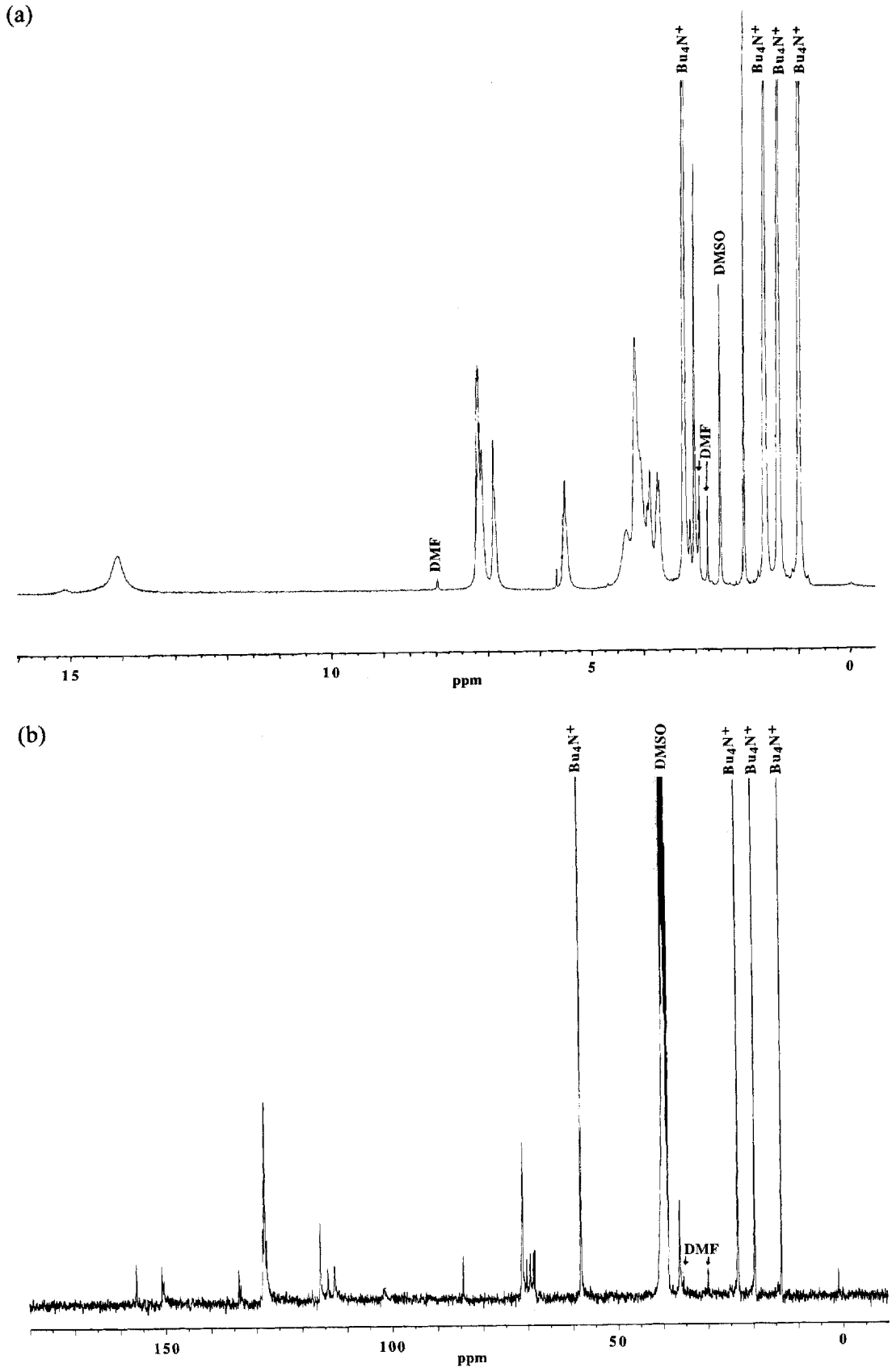

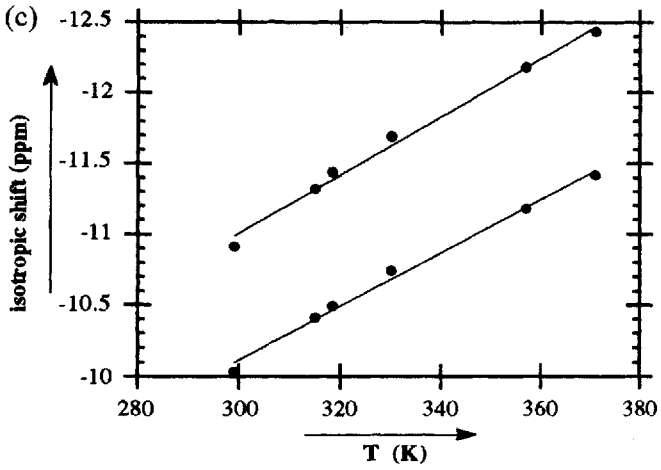

Figure 4. Mössbauer spectrum of cluster complex **4** measured at room temperature (a) and at 77 K (b); Mössbauer spectrum of $[Fe_4S_4Cl_4](n\text{-}Bu_4N)_2$, measured at room temperature (c)

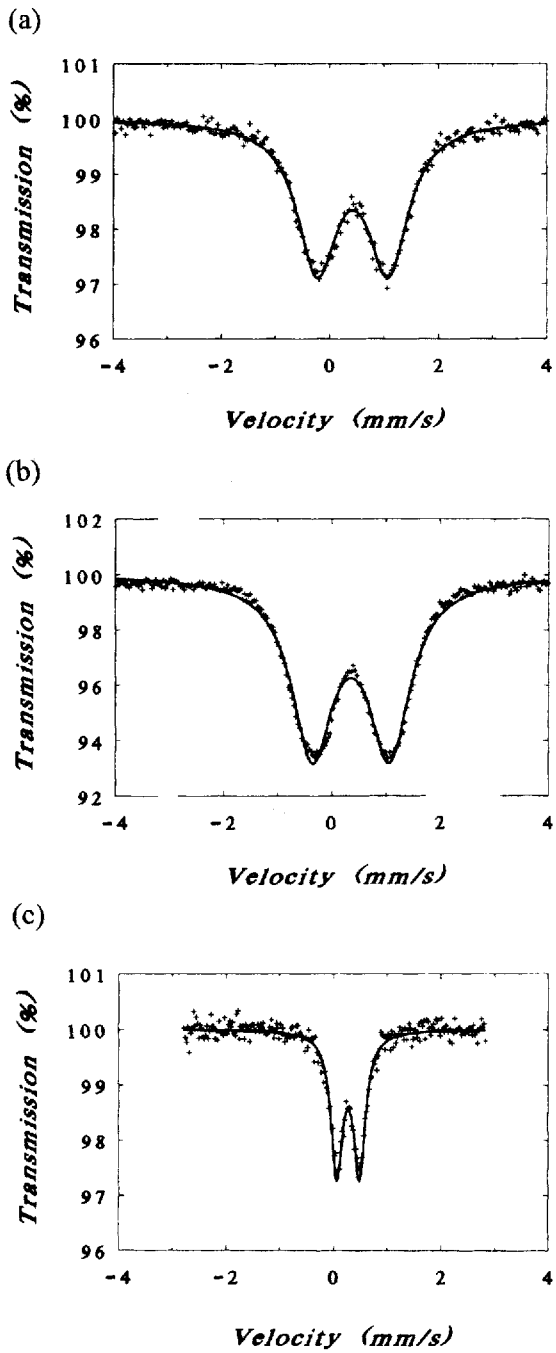

ting is found to depend on the counterion used[38]. The presence of such slightly different electronic environments does not contradict the conclusion from the Mössbauer spectra that **4** contains an intact [4Fe-4S] cluster.

Electrochemical Measurements

The formation of **4** from **3** and $[Fe_4S_4Cl_4]^{2-}$ was followed by monitoring the disappearance of the $2^-/3^-$ reduction wave of the latter cluster. Although the ^{1}H-NMR spectrum indicated that the correct product had been formed, hardly any electrochemical response was seen for the newly formed complex. However, the peak current improved upon addition of Ba^{2+} ions (as their ClO_4^- salt). Similar effects of cations have been noted[26] for a variety of negatively charged metalloproteins in water, e.g. ferredoxins and plastocyanin, but not for positively charged proteins, e.g. cytochrome c[39]. The effects of cations as promoters of the electrochemical response of redox proteins have been thoroughly investigated by Hill and Armstrong[40]. In order to investigate the effects of Ba^{2+} and Na^+ ions (as their ClO_4^- salts) on the electrochemistry of **4** in detail, we used four different electrodes in our cyclic voltammetry study: platinum, gold and two different types of carbon electrodes, viz. pyrolytic graphite edge (PGE) and pyrolytic graphite basal (PGB). The results are presented in Table 1.

Without promoter only the carbon electrodes show some response. When Ba^{2+} is added in low concentration (5 mM), the peak currents for all four electrodes increase. A further increase in the concentration of the promoter improves the (electro)chemical reversibility of the system for all electrodes as judged from the $i_{p,c}/i_{p,a}$ value (or i_b/i_f, the ratio of maximum backward and forward currents) and the peak separation, ΔE_p[41]. The best results are obtained with the carbon electrodes, for which $i_{p,c}/i_{p,a}$ approaches 0.80. The optimum Ba^{2+} concentration for both the current response and the reversibility is approximately 25 mmol l^{-1}. Ba^{2+} has a larger effect than Na^+[40]. For the latter ion, the concentrations required to observe an improvement in the electrochemistry are at least 25–50 times higher than for Ba^{2+}. Such high Na^+ concentrations result in the precipitation of **4**. As can be seen from Table 1, Ba^{2+} also acts as a modulator, shifting the $2^-/3^-$ reduction potential by +70 mV. For the PGE and Pt electrodes a cathodic-anodic peak separation close to the theoretical value for a one-electron process is observed (ca. 65 mV). The peak separation for the PGB electrode is 42 mV. This low value suggests that **4** becomes absorbed on the surface of this electrode. Interaction between the large aromatic surfaces present on the basal plane of the PGB electrode and the aromatic groups in **4** may be the reason for this adsorption.

Table 1. Cyclic voltammetry data obtained for complex **4** under various conditions[a]

electrode	[modulator]	$i_{p,a}$ [b]	$i_{p,c}$ [b]	$i_{p,c}/i_{p,a}$	$E_{1/2}$ (V)	ΔE_p (mV)
Pt	–	–	–	–	–	–
Au	–	–	–	–	–1.70	110
PGB	–	1.00	0.35	0.35	–1.69	58
PGE	–	1.15	–	–	–1.70	75
Pt	5 mM Ba^{2+}	3.9	1.1	0.28	–1.67	95
Au	5 mM Ba^{2+}	8.9	2.5	0.28	–1.68	116
PGB	5 mM Ba^{2+}	1.8	1.1	0.61	–1.67	42
PGE	5 mM Ba^{2+}	2.7	2.3	0.85	–1.67	58
Pt	10 mM Ba^{2+}	4.8	2.2	0.46	–1.66	75
Au	10 mM Ba^{2+}	8.4	4.1	0.49	–1.67	95
PGB	10 mM Ba^{2+}	2.4	1.6	0.67	–1.66	42
PGE	10 mM Ba^{2+}	4.2	3.2	0.76	–1.66	65
Pt	25 mM Ba^{2+}	4.5	1.9	0.42	–1.65	72
Au	25 mM Ba^{2+}	9.1	4.6	0.51	–1.65	85
PGB	25 mM Ba^{2+}	3.3	2.3	0.70	–1.65	41
PGE	25 mM Ba^{2+}	5.2	4.1	0.79	–1.64	68
Pt	50 mM Ba^{2+}	4.7	1.5	0.32	–1.64	85
Au	50 mM Ba^{2+}	7.3	2.7	0.37	–1.63	93
PGB	50 mM Ba^{2+}	3.2	2.2	0.69	–1.64	43
PGE	50 mM Ba^{2+}	4.7	2.9	0.62	–1.63	60
Pt	100 mM Na^+	–	–	–	–	–
Au	100 mM Na^+	–	–	–	–	90
PGB	100 mM Na^+	1.2	0.2	0.17	–1.69	73
PGE	100 mM Na^+	2.9	1.1	0.38	–1.69	60
Pt	500 mM Na^+	4.9	2.0	0.41	–1.66	75
Au	500 mM Na^+	9.7	3.5	0.36	–1.66	72
PGB	500 mM Na^+	3.0	1.0	0.33	–1.66	50
PGE	500 mM Na^+	4.8	2.1	0.44	–1.65	48

[a] $2^{-}/3^{-}$ reduction of **4** in DMF solution; a Pt-auxiliary electrode and an Ag/AgCl reference electrode were used; 0.1 M^{-1} tetrabutylammonium hexafluorophosphate (TBAH) was added as the supporting electrolyte; potentials are given vs. Fc^+/Fc in DMF. – [b] Arbitrary units.

In the presence of Ba^{2+}, a plot of the peak current (i_{pc}) vs. the square root of the scan rate (ν) shows a linear response (see Figure 5). This indicates that a process controlled by linear diffusion is responsible for mass transport to the electrode[42], and that no adsorption processes interfere. Comparison of the cyclic voltammograms before (Figure 6a) and after (Figure 6b) the addition of the promoter leads to the conclusion that the number of electroactive sites on the electrode increases when the latter is added. The sigmoidal curve in Figure 6a is typical of mass transport to the electrode controlled by radial diffusion, resulting from a low density of electroactive sites[42,43]. An increase in the concentration of Ba^{2+} leads to an increase in the number of electroactive sites and hence to a change in diffusion profile, clearly demonstrated by the $i_{p,c}$ vs. $\nu^{1/2}$ plot.

It should be noted that, even after correction for the difference in reference[44], the $E_{1/2}$ of -1.7 V vs. Fc^+/Fc for **4** in DMF is very much more negative than the $E_{1/2}$ values for ferredoxins vs. NHE in water (see the Introduction). Such differences between synthetic iron-sulfur clusters and ferredoxins have been noted before[45] and were ascribed to effects of solvent and protein environment. We conclude that while the encapsulation of the [4Fe-4S] cluster by **3** mimics the asymmetry of clusters in proteins and the effect

Figure 5. Top: Cyclic voltammograms of **4** recorded as a function of the scan rate ν: 25 mV s^{-1} (1); 50 mV s^{-1} (2); 100 mV s^{-1} (3); 200 mV s^{-1} (4); 400 mV s^{-1} (5). Bottom: Plot of the peak curent, in arbitrary units, for the $2^{-}/3^{-}$ reduction of **4** vs. the square root of the scan rate, $\nu^{1/2}$, verifying the predominance of linear diffusion

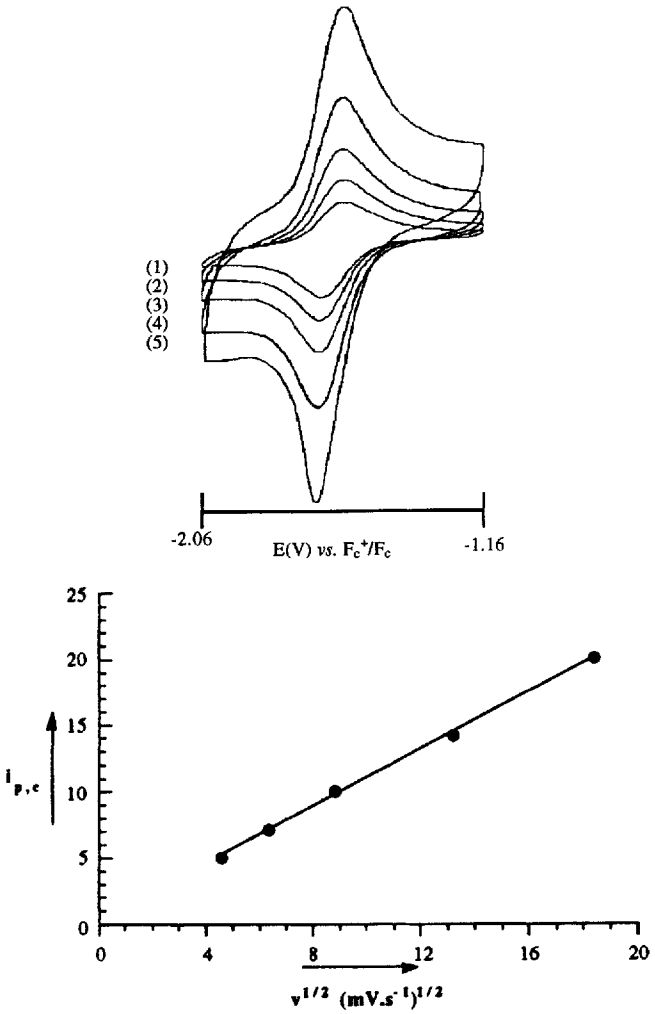

Figure 6. Cyclic voltammograms (PGE electrode) of cluster compound **4** in DMF solution (scan rate 100 mV s^{-1}) before (A) and after (B) the addition of 20 mM Ba^{2+} as the perchlorate salt

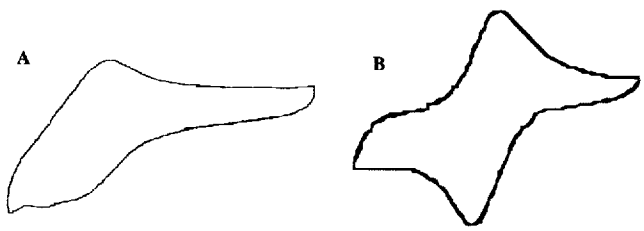

of promoter ions in its cluster complex, it does not resemble the protein shell in its tuning of the redox potential.

Scanning Tunneling Microscopy (STM) and Scanning Electron Microscopy (SEM)

As the nature of the electrode and the promoter apparently play an important role in the reduction process of **4**, we carried out an STM/SEM study on the PGE and the

PGB electrodes. Both materials were given the same surface treatment as the electrodes used in the actual electrochemical measurements, viz. a polishing procedure with 0.3-μm aluminium oxide, followed by sonication. This procedure is expected to increase the number of oxidized carbon surface groups, e.g. phenolate, carboxylate, etc.[46], which have a beneficial effect on the electrochemical current response. It was difficult to obtain a stable tunnelling current at high resolutions for the PGE electrode used in this study, and it was impossible to achieve atomic resolution. The tunnelling current was less noisy for the PGB electrode and some places showed atomic resolution. Difficulties in obtaining atomic resolution at reactive carbon sites (e.g. at the edges of etch pits on highly oriented pyrolytic graphite, HOPG) have been reported before in the literature[47]. Comparison of the STM images of PGE and PGB electrodes revealed that the total surface area of the former is larger, that its surface is highly corrugated and that it has a larger variation in height. The typical variations in height over a 200 × 200 Å area are 0–30 Å for PGB (Figure 7, left) and 0–70 Å for PGE (Figure 8).

The possible deposition of Ba^{2+} on the electrode surface was investigated with PGE, PGB, and highly oriented pyrolytic graphite (HOPG) electrodes. Cyclic voltammograms

Figure 7. Top: Intensity STM image of a PGB electrode before (left) and after (right) using the electrode in a Ba^{2+}-containing solution: a 200 × 200 Å area is shown. Middle: Line STM imaging of the same surfaces. Bottom: Cross-section depth profile: the arrows in the line plot denote the orientation of the profile

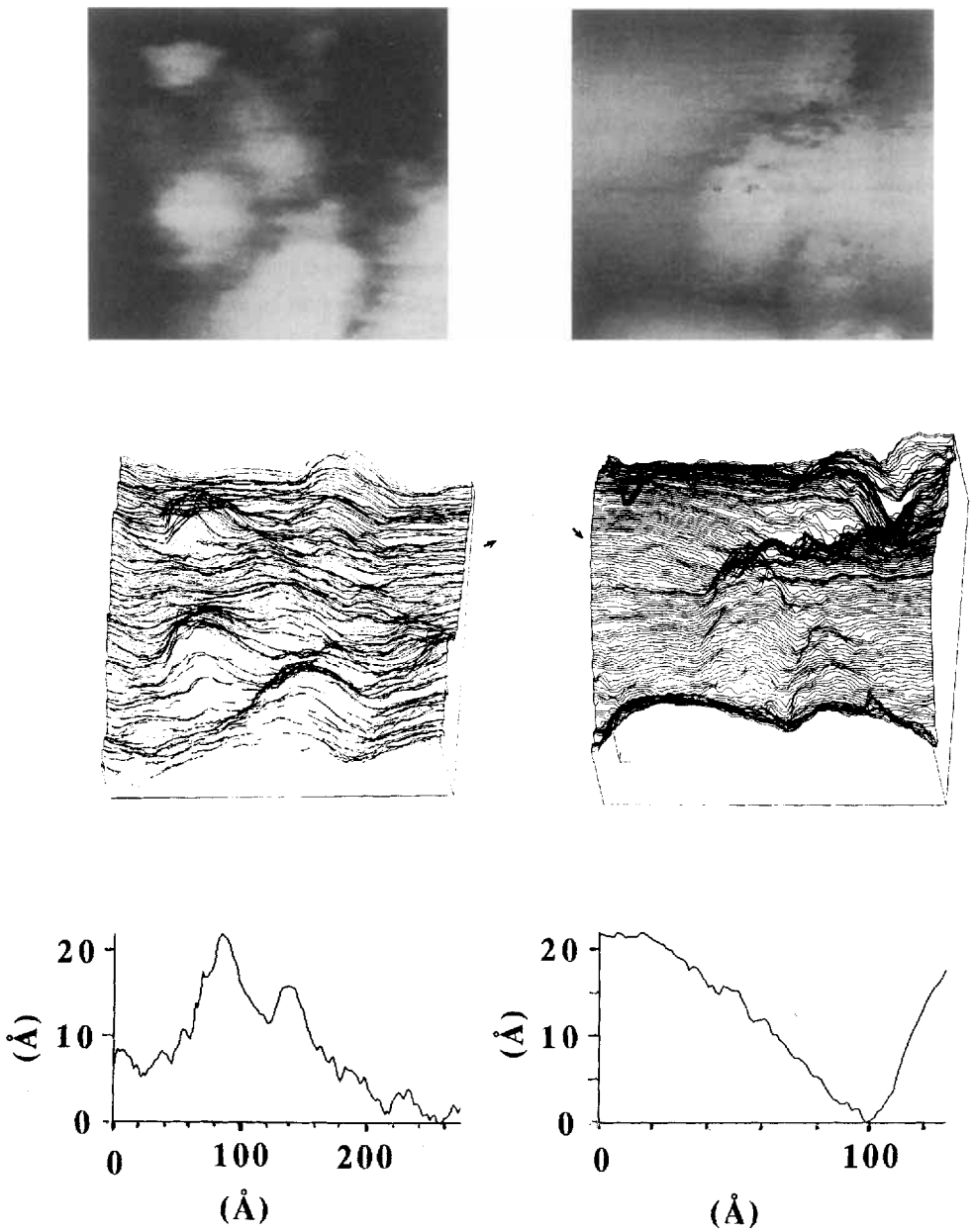

Figure 8. Intensity (left) and line (right) STM images of a PGE electrode: surface area 200 × 200 Å. Shown on the bottom is a cross-section depth profile of the STM image: the arrows in the line plot denote the orientation along which the profile was taken

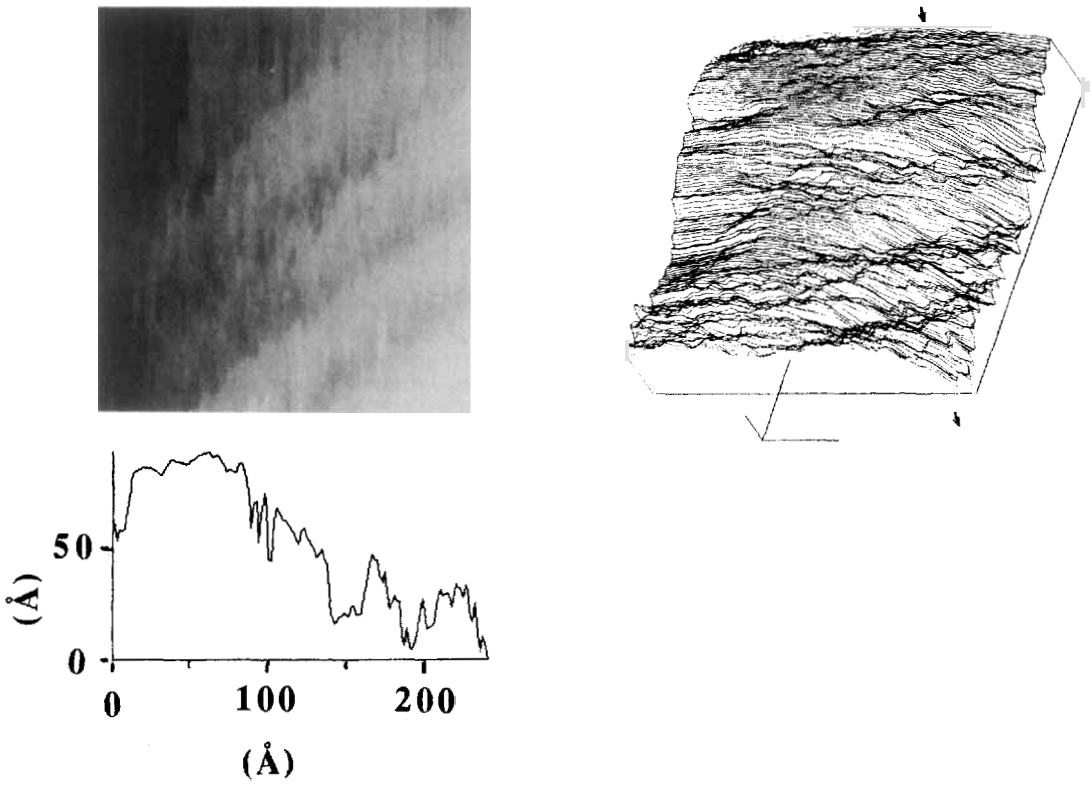

with these electrodes were run under identical conditions with solutions containing Ba^{2+} but no cluster complex **4**. After the electrodes had been removed from the solutions, STM pictures were taken. Comparison with the images obtained from electrodes that had not been exposed to Ba^{2+} gave no indications for major changes in the overall topography of the electrode surface (not shown). However, SEM images of the HOPG electrode showed that the surface was covered with non-carbonic material, which according to the X-ray backscattering spectrum (see Figure 9) contained Ba together with Cl. Our conclusion is therefore that during the electrochemical measurements Ba^{2+} is adsorbed onto the negatively charged HOPG electrode.

Figure 9. X-ray backscattering spectrum of an HOPG electrode used in a cyclic voltammetric experiment with $Ba(ClO_4)_2$

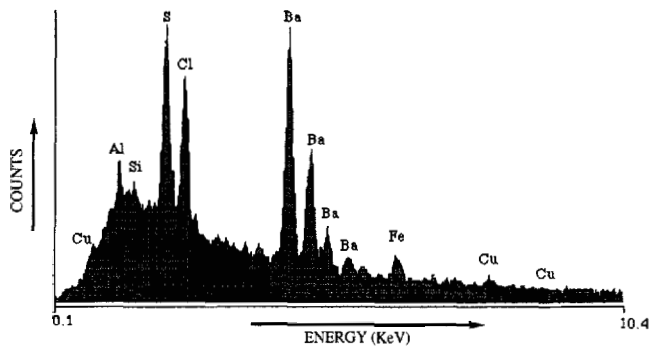

Type of Interaction of 4 with the Electrode Surface

Apart from facilitating electron transfer by creating electroactive sites, Ba^{2+} ions may also assist in orienting molecules of **4** into the correct position with respect to the electrode surface. Complex **4** has a dipole moment with a negative charge on top. Without the addition of Ba^{2+} ions the electrode surface will be negatively charged and **4** will tend to approach it with its negative side away from the surface, thus minimizing the electrostatic repulsion. In addition, π-π interaction between the aromatic groups on the convex side of **4** and the aromatic arrays on the surface of the graphite electrodes could stabilize a "tail-first" docking (T-shaped π-π interactions) or a "sideways" docking (stacked π-π interaction, Figure 10a and b)[48]. In the former case, **4** docks on the electrode with its Fe_4S_4 **core** away from the surface; in the latter case the molecule lies flat on the electrode. In both situations the interactions between the redox centre and the electrode surface do not seem to be favourable for electron transfer. Upon addition of Ba^{2+}, the polarity on the electrode surface changes and a "head-first" docking is more likely (Figure 10c). If this explanation is correct, then more symmetric clusters such as $[Fe_4S_4X_4]^{2-}$ (X = S-alkyl, S-aryl or halogen) should experience no effect of Ba^{2+} ions. To test this we investigated the electrochemical behaviour of a small series of simple cluster compounds $[Fe_4S_4X_4]^{2-}$ (X = Cl, SPh and SCH_2CH_2OH) in the presence of Ba^{2+}. Three different types of electrodes were used.

The general trend of the experiments was that the addition of Ba^{2+} had no effect, except when X = SCH_2CH_2OH in which case Ba^{2+} had a negative effect. Probably this cluster complex is able to form a relatively tight ion pair with Ba^{2+} ions due to the presence of the hydroxyl groups. This might result in a repulsion of the cluster from the Ba^{2+}-coated electrode surface.

Figure 10. Possible interactions of **4** with the electrode surface: "face-to-face" docking (a); "tail-first" docking (b); and "head-first" docking (c)

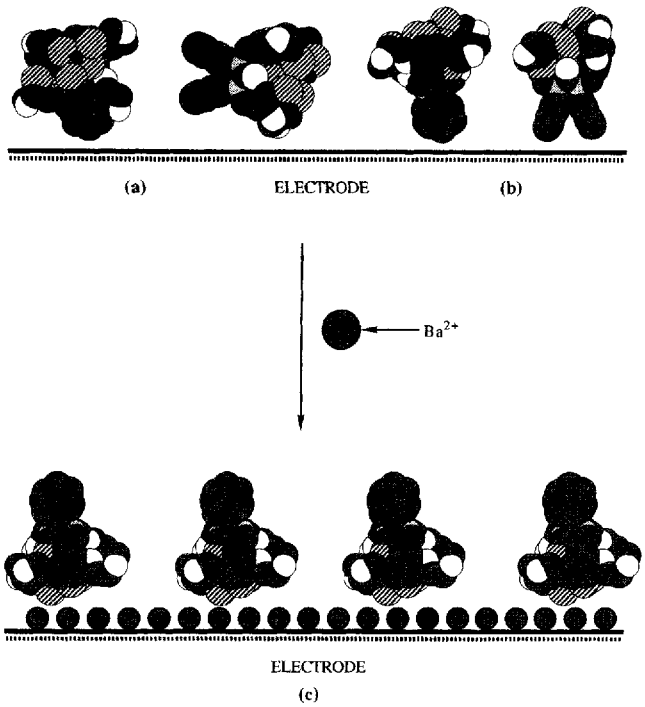

In summary, the electrochemical results presented here can be explained by assuming a preferred mode of docking of **4** on the electrode surface (depicted in Figure 10). Before the addition of Ba^{2+} ions, a random distribution of the orientations of the cluster complexes is likely. Upon addition of the promoter, this distributon changes and a "head-first" docking mode becomes predominant. In this way, the cluster core is more capable of accepting or donating electrons, and an increase in current is observed.

Conclusions

In this paper we have presented a novel ligand system, containing a rigid cavity and four spacer arms, terminating with thiol groups. The ligand is capable of semi-encapsulating an $[Fe_4S_4]^{2-}$ cluster in an asymmetric way. As a result, the cluster complex has a dipole and exhibits electrochemical behaviour previously only encountered for metalloproteins. It is proposed that upon addition of a promoter (Ba^{2+}), the dipole orients itself in such a why that the complex docks in a favourable, "head-first" mode, allowing electron transfer. Such an orientational effect of a promoter has also been observed[38] with proteins like rubredoxin[49], azurin[50], and flavodoxin[51]. These proteins possess a quite pronounced asymmetry both in terms of the location of the redox centres and (in varying degrees) in terms of the distribution of charged and hydrophobic surface residues[38]. The mimic **4** is similar in this respect. Ba^{2+} ions also modulate the reduction potential of **4**, shifting it by +70 mV. Finally, the addition of Ba^{2+} also changes the type of diffusion to the electrode, viz. from radial to linear, supporting the microscopic model proposed by Hill and Armstrong[40].

The authors thank Drs. *F. Mulders* and *R. Thiele* (University of Leiden) for Mössbauer spectra, and Prof. *H. van Kempen* and Prof. *J. J. Steggerda* for stimulating discussions.

Experimental Section

General Methods: All manipulations involving compounds with a [4Fe-4S] core were carried out under anaerobic conditions. All solvents were dried prior to distillation under dinitrogen. Diethylether was distilled from sodium. Dichloromethane and acetonitrile were distilled from calcium hydride. DMF was stored over 4-Å molecular sieves and distilled at reduced pressure. UV/Vis spectra were recorded on a Perkin-Elmer Lambda 5 spectrometer. ^{1}H- and ^{13}C-NMR spectra were recorded on a Bruker WH90 or Bruker WM-400 instrument. FAB-MS specta were recorded on a VG 7070E instrument using 3-nitrobenzyl alcohol as a matrix. IR spectra were measured on a Perkin-Elmer 1720X instrument. Melting points were measured on a Reichert-Jung hot stage mounted on a microscope and are reported uncorrected. Pyrolytic graphite electrodes (Lorraine le Carbon) were prepared according to the method described by Hill and Armstrong[39]. The electrodes were polished before use, using a 0.3-μm aluminium oxide slurry (BDH) followed by sonication. All electrochemical measurements were carried out in a glove box under a dinitrogen atmosphere containing less than 10 ppm of dioxygen. STM images were obtained on a home-built device, operated in the height image (constant current) mode under ambient conditions as described elsewhere[52,53]. PtIr was used as the tip material. Typical operating conditions are: bias voltage = −50 mV; set point current = 80 pA.

5,7,12,13b,13c,14-Hexahydro-1,4,8,11-tetrakis[2-(2-chloroethoxy)ethoxy]-13b,13c-diphenyl-6H,13H-5a,6a,12a,13a-tetraazabenz[5,6]azuleno[2,1,8-ija]benz[f]azulene-6,13-dione (**1**): This compound was prepared according to a procedure[24] described by us previously.

5,7,12,13b,13c,14-Hexahydro-1,4,8,11-tetrakis{2-[2-(thioacetyl)-ethoxy]ethoxy}-13b,13c-diphenyl-6H,13H-5a,6a,12a,13a-tetraazabenz[5,6]azuleno[2,1,8-ija]benz[f]azulene-6,13-dione (**2**): In a Schlenk vessel and under a dinitrogen atmosphere, 995 mg (3.05 mmol) of Cs_2CO_3 was dispersed in 5 ml of degassed DMF. To this suspension was added 480 mg (6.32 mmol) of freshly distilled thioacetic acid. After the CO_2 evolution had ceased, 1 g (1.01 mmol) of **1** was added, together with a catalytic amount of NaI. The Schlenk vessel was wrapped with aluminium foil to block out light and was heated at 60 °C for 18 h. In most cases a dark-yellow to red colour developed. After cooling to room temperature 70 ml of dichloromethane was added and the reaction mixture was washed with brine (6×). The organic layer was separated, dried (Na_2SO_4), filtered and concentrated under reduced pressure. The resulting solid material was purified by column chromatography on silica 60H (eluent 1% MeOH in $CHCl_3$) to yield **2** as a white solid (730 mg, 63%, pure according to TLC and ^{1}H NMR). The compound was recrystallized from acetone. – M.p. 190 °C. – R_f (TLC, eluent 1% MeOH in $CHCl_3$): 0.15. – ^{1}H NMR (400 MHz, $CDCl_3$): δ = 2.33 [s, 12H, $SC(O)CH_3$], 3.12 (t, 8H, OCH_2CH_2S), 3.70 (m, 8H, OCH_2CH_2S), 3.80 (m, 8H, OCH_2CHHO and $NCHH$), 3.89

(m, 4H, OCH_2CHHO), 3.99 (m, 4H, $OCHHCH_2O$), 4.08 (m, 4H, $OCHHCH_2O$), 5.53 (d from AB, 4H, NCH*H*), 6.67 (s, 4H, Xy*H*), 7.09 (m, 10H, PhH). – ^{13}C NMR ($CDCl_3$): δ = 29.02 (OCH_2CH_2S), 30.52 [$CH_3C(O)S$], 37.06 (NCH_2Ar), 69.82 (OCH_2CH_2O and OCH_2CH_2S), 70.04 (OCH_2CH_2O), 85.18 [NC(N)Ar], 114.57 (XyC), 128.17 (ArC), 128.32 (ArC), 128.42 (ArC), 134.08 (ArC), 150.85 (ArC), 157.75 [NC(O)N], 195.50 [SC(O)CH_3]. – IR (KBr): $\tilde{\nu}$ = 3035–2929 cm^{-1} (ArH, CH_2), 1706 (C=O), 1686 (R–CO–SR), 1123 (COC). – FAB-MS; *m/z*: 1148 [M + H^+]. – $C_{56}H_{66}N_4O_{14}S_4$: calcd. C 59.17, H 6.04, N 5.41, S 12.39; found C 58.42, H 5.68, N 4.85, S 11.43.

5,7,12,13b,13c,14-Hexahydro-1,4,8,11-tetrakis[2-(2-mercaptoethoxy)ethoxy]13b,13c-diphenyl-6H,13H-5a,6a,12a,13a-tetraazabenz[5,6]azuleno[2,1,8ija]benz[f]azulene-6,13-dione (**3**): Under a dinitrogen atmosphere 100 mg (0.087 mmol) of **2** was dissolved in 2 ml of dichloromethane. To this solution was added 4.1 ml of a 0.1 M solution of sodium methoxide in methanol. The homogeneous solution was stirred for 25 min at ambient temperature and subsequently the solvent was removed under reduced pressure. The solid material was redissolved in degassed water and the solution was acidified using a 2 N aqueous HCl solution. The mixture was extracted with chloroform (3×) and the combined organic layers were dried ($MgSO_4$), filtered, and concentrated under reduced pressure to yield **3** as a white solid (78 mg, 92%). – M.p. 224 °C. – R_f (TLC, eluent 2% MeOH in $CHCl_3$): 0.1. – ^1H NMR ($CDCl_3$): δ = 1.62 (t, 4H, S*H*), 2.67 (q, 8H, CH_2S), 3.5–4.1 (28H, $OCH_2CH_2OCH_2$, ArCHHN), 5.50 (d, 4H, ArCH*H*N), 6.58 (s, 4H, Xy*H*), 7.01 (s, 10H, Ph*H*). – ^{13}C NMR ($CDCl_3$): δ = 24.38 (CH_2S), 37.02 (NCH_2Ar), 69.72 (CH_2OCH_2), 69.92 (OCH_2CH_2S), 72.97 ($ArOCH_2$), 85.19 [NC(N)Ar], 114.25 (XyC), 128.14, 128.46 (XyC and ArC), 133.86 (ArC), 150.72 (ArC), 157.72 [NC(O)N]. – IR (KBr): $\tilde{\nu}$ = 2924 cm^{-1} (ArH), 2857 (CH_2), 2542 (SH), 1708 (C=O), 1050 (COC) cm^{-1}. – FAB-MS; *m/z*: 979 [M + $H]^+$. – $C_{48}H_{58}N_4O_{10}S_4$ · MeOH: calcd. C 58.87, H 5.97, N 5.72, S 13.10; found C 59.34, H 5.86, N 5.64, S 12.77.

Complex **4**. – *Method A:* Under a dinitrogen atmosphere 100 mg (0.087 mmol) of **2** was dissolved in 2 ml of dichloromethane. To this solution was added 4.1 ml of a 0.1 M solution of sodium-methoxide in methanol. The homogeneous solution was stirred for 25 min. at ambient temperature and subsequently the solvent was removed under reduced pressure. The solid material was suspended in DMF and to this suspension was added 85 mg (0.087 mmol) of $[Fe_4S_4Cl_4]$ · $(n\text{-}Bu_4N)_2$. The mixture was stirred for 12 h. At regular time intervals a sample was taken which was analysed with cyclic voltammetry and differential pulse polarography to monitor the progress of the reaction. After the starting material had disappeared, diethyl ether was added to precipitate the product. The black precipitate was washed with acetonitrile to remove unreacted $[Fe_4S_4Cl_4]^{2-}$ and by-products and was recrystallized from DMF/diethyl ether.

Method B: To a homogeneous solution of 100 mg (0.1 mmol) of **3** and 100 mg (0.1 mmol) of $[Fe_4S_4Cl_4]$ · $(n\text{-}Bu_4N)_2$ in 100 ml of DMF, 4 ml of a 0.1 M solution of $n\text{-}Bu_4NOH$ in methanol was added while stirring. From this point on, the same procedure as described for method A was followed. **4**: – ^1H NMR ([D_6]DMSO, T = 353 K, Figure 3a): δ = 0.96 (m, 24H, $NCH_2CH_2CH_2CH_3$), 1.37 (m, 16H, $NCH_2CH_2CH_2CH_3$), 1.63 (m, 16H, $NCH_2CH_2CH_2CH_3$), 3.18 (m, 16H, $NCH_2CH_2CH_2CH_3$), 3.69–4.50 (m, 28H, $OCH_2CH_2OCH_2$ and NCHH), 5.50 (s, 4H, NCH*H*), 6.87 (s, 4H, XyH), 7.10, 7.18 (m, 10H, Ph*H*), 14.08, 15.11 (br., 8H, OCH_2CH_2S). Some solvent peaks are indicated in the spectrum; unknown solvent peaks, due to the glove-box atmosphere, are observed at δ = 2.03 and 2.98. – ^{13}C NMR ([D_6]DMSO, T = 308 K, Figure 3b): δ = 13.73 ($NCH_2CH_2CH_2CH_3$), 19.69 ($NCH_2CH_2CH_2CH_3$), 23.42 ($NCH_2CH_2CH_2CH_3$), 36.33 (NCH_2Ar), 58.22 ($NCH_2CH_2CH_2CH_3$), 68.47, 68.67, 69.49, 70.31, 71.21 (CH_2OCH_2, $ArOCH_2$), 84.37 [NC(N)Ar], 102.3 (CH_2S and/or CH_2CH_2S), 114.30, 115.95 (XyC), 127.73, 128.23, 128.50, 128.60 (ArC), 133.46, 133.88 (XyC), 150.40, 150.83 (XyC), 156.40 [NC(O)N]. – UV/Vis (DMF): λ_{max}/nm (ε/l mol^{-1} cm^{-1}) for $[Fe_4S_4(4)]$ · $\{nBu_4N\}_2$: 297 (23300), 418 (17200). – FAB-MS (negative mode); *m/z*: 1270 [M – Fe]

[1] J. B. Vincent, G. L. Olivier-Lilley, B. A. Averill, *Chem. Rev.* **1990**, *90*, 1447.
[2] *Electron Transport and Oxygen Utilization* (Ed.: C. Ho), Macmillan Press, London–Basingstoke, **1982**.
[3] *Hemoglobin and Oxygen Binding* (Ed.: C. Ho), Macmillan Press, London–Basingstoke, **1982**.
[4] S. E. V. Phillips, *Nature* **1978**, *273*, 726.
[5] M. F. Perutz, *Annu. Rev. Biochem.* **1979**, *48*, 327.
[6] R. E. Stenkamp, L. C. Sieker, L. H. Jensen, *J. Am. Chem. Soc.* **1984**, *106*, 618.
[7] *Iron-Sulfur Proteins* (Ed.: W. Lovenberg), Academic Press, New York, **1973**, vols. I and II.
[8] V. Petrouleas, J. J. Brand, K. G. Parrett, J. Golbeck, *Biochemistry* **1989**, *28*, 8980.
[9] M. C. W. Evans in *Iron-Sulfur proteins* (Ed.: T. G. Spiro), Interscience, New York, **1982**, vol. 4, chapter 6.
[10] *Inorganic Nitrogen Metabolism* (Eds.: W. R. Ullrich, P. J. Aparicio, P.J. Syrett, F. Castillo), Springer-Verlag, Berlin–Heidelberg, **1987**.
[11] T. Ohnishi, J. C. Salerno in *Iron-Sulfur proteins* (Ed.: T. G. Spiro), Interscience, New York, **1982**, vol. 4, chapter 7.
[12] G. Backes, Y. Mino, T. M. Loehr, T. E. Meyer, M. A. Cusanovich, W. V. Sweeney, E. T. Adman, J. Sanders-Loehr, *J. Am. Chem. Soc.* **1991**, *113*, 2055.
[13] A. Nakamura, N. Ueyama, *Adv. Inorg. Chem.* **1989**, *33*, 39.
[14] N. Ueyama, A. Kajiwara, T. Terakawa, S. Ueno, A. Nakamura, *Inorg. Chem.* **1985**, *24*, 4700.
[15] Y. Kuroda, Y. Sasaki, Y. Shiroiwa, I. Tabushi, *J. Am. Chem. Soc.* **1988**, *110*, 4049.
[16] Y. Okuno, K. Uoto, Y. Sasaki, O. Yonemitsu, T. Tomohiro, *J. Chem. Soc., Chem. Commun.* **1987**, 874.
[17] Y. Okuno, K. Uoto, T. Tomohiro, M.-T. Youinou, *J. Chem. Soc., Dalton Trans.* **1990**, 3375.
[18] T. D. P. Stack, R. H. Holm, *J. Am. Chem. Soc.* **1987**, *109*, 2546.
[19] T. D. P. Stack, R. H. Holm, *J. Am. Chem. Soc.* **1988**, *110*, 2484.
[20] G. P. F. van Strijdonck, J. A. E. H. van Haare, J. G. M. van der Linden, J. J. Steggerda, R. J. M. Nolte, *Inorg. Chem.* **1994**, *33*, 999.
[21] J. W. H. Smeets, R. P. Sybesma, F. G. M. Niele, A. L. Spek, W. J. J. Smeets, R. J. M. Nolte, *J. Am. Chem. Soc.* **1987**, *109*, 928.
[22] R. P. Sybesma, W. P. Bosman, R. J. M. Nolte, *J. Chem. Soc., Chem. Commun.* **1991**, 885.
[23] H. K. A. C. Coolen, P. W. N. M. van Leeuwen, R. J. M. Nolte, *Angew. Chem., Int. Ed. Engl.* **1992**, *31*, 905.
[24] C. F. Martens, R. J. M. Klein Gebbink, M. C. Feiters, R. J. M. Nolte, *J. Am. Chem. Soc.* **1994**, *116*, 5667.
[25] C. F. Martens, H. L. Blonk, T. Bongers, J. G. M. van der Linden, G. Beurskens, P. T. Beurskens, J. M. M. Smits, R. J. M. Nolte, *J. Chem. Soc., Chem. Commun.* **1991**, *22*, 1623.
[26] F. A. Armstrong, H. A. O. Hill, B. N. Oliver, N. J. Walton, *J. Am. Chem. Soc.* **1984**, *106*, 921.
[27] J. W. H. Smeets, H. C. Visser, V. E. M. Kaats-Richter, R. J. M. Nolte, *Recl. Trav. Chim. Pays-Bas.* **1990**, *109*, 147.
[28] B. Strijdveen, R. M. Kellogg, *J. Org. Chem.* **1986**, *51*, 3664.
[29] T. D. P. Stack, J. A. Weigel, R. H. Holm, *Inorg. Chem.* **1990**, *29*, 3745.
[30] *Spektroskopische Methoden in der organischen Chemie* (Eds.: M. Hesse, H. Meier, H. B. Zeeh), Georg Thieme Verlag, Stuttgart, 4th print, **1991**.
[31] M. A. Bobrik, L. Que, Jr., R. H. Holm, *J. Am. Chem. Soc.* **1974**, *96*, 285.
[32] J. M. Berg, R. H. Holm in *Iron-Sulfur proteins* (Ed.: T. G. Spiro), Interscience, New York, **1982**, vol. 4, chapter 1.
[33] G. B. Wong, M. A. Bobrik, R. H. Holm, *Inorg. Chem.* **1978**, *17*, 578.

[34] R. W. Johnson, R. H. Holm, *J. Am. Chem. Soc.* **1978**, *100*, 5338.
[35] R. H. Holm, W. D. Phillips, B. A. Averill, J. J. Mayerle, T. Herskovitz, *J. Am. Chem. Soc.* **1974**, *96*, 2109.
[36] G. Christou, C. D. Garner, M. G. B. Drew, R. Cammack, *J. Chem. Soc., Dalton Trans.* **1981**, 1550.
[37] T. J. Ollerenshaw, S. Bristow, B. N. Anand, C. D. Garner, *J. Chem. Soc., Dalton Trans.* **1986**, 2013.
[38] D. J. Evans, A. Hills, D. L. Hughes, G. J. Leigh, A. Houlton, J. Silver, *J. Chem. Soc., Dalton Trans.* **1990**, 2735.
[39] F. A. Armstrong, H. A. O. Hill, *Acc. Chem. Res.* **1988**, *21*, 407.
[40] F. A. Armstrong, P. A. Cox, H. A. O. Hill, V. J. Lowe, B. N. Oliver, *J. Electroanal. Chem.* **1987**, *217*, 331.
[41] A. J. Bard, L. J. Faulkner, *Electrochemical Methods, Fundamentals and Applications*, John Wiley & Sons, Inc., New York, **1980**.
[42] F. A. Armstrong, A. M. Bond, H. A. O. Hill, B. N. Oliver, I. S. M. Psalti, *J. Am. Chem. Soc.* **1989**, *111*, 9185.
[43] A. M. Bond, H. A. O. Hill in *Metal Ions in Biological Systems*, Marcel Dekker, Inc., New York, **1991**, vol. 27, 431.
[44] It is difficult to compare potentials in water and organic solvents because of the liquid junction potential that is introduced when a saturated calomel electrode (SCE) is transferred from water to an organic solvent (cf. ref.[41]). Using the following data: $E_{1/2}$ for Fc^+/Fc vs. Ag/AgCl (0.1 M LiCl in DMF) in DMF: 0.76 V; $E_{1/2}$ for $FcCOOH^+$/FcCOOH (ferrocene carboxylic acid) vs. Ag/AgCl in DMF: 0.96 V; $E_{1/2}$ for $FcCOOH^+$/FcCOOH vs. SCE in water: 0.29 V; $E_{1/2}$ for SCE vs. NHE: −0.24 V (ref.[41]), we can calculate that a value of −1.70 V for $E_{1/2}$ of **4** vs. Fc^+/Fc in DMF means −1.90 V vs. $FcCOOH^+$/FcCOOH in DMF and water, and −1.85 V vs. NHE in water.
[45] B. V. DePamphilis, B. A. Averill, T. Herkovitz, L. Que, Jr., R. H. Holm, *J. Am. Chem. Soc.* **1974**, *96*, 4159.
[44] J. Scheurs, E. Barendrecht, *Recl. Trav. Chim. Pays-Bas* **1984**, *103*, 205.
[45] H. Chang, A. J. Bard, *J. Am. Chem. Soc.* **1991**, *113*, 5588.
[46] W. L. Jorgenson, D. L. Severance, *J. Am. Chem. Soc.* **1990**, *112*, 4768.
[47] K. D. Watenpaugh, L. C. Sieker, L. H. Jensen, *J. Mol. Biol.* **1979**, *131*, 509.
[48] E. T. Adman, L. H. Jensen, *Isr. J. Chem.* **1981**, *21*, 8.
[49] W. W. Smith, R. M. Burnett, G. D. Darling, M. L. Ludwig, *J. Mol. Biol.* **1977**, *117*, 195.
[50] R. Czajka, C. G. J. Koopal, M. C. Feiters, J. W. Gerritsen, R. J. M. Nolte, H. van Kempen, *Bioelectrochem. Bioenerg.* **1992**, *29*, 47.
[51] C. G. J. Koopal, M. C. Feiters, R. J. M. Nolte, B. de Ruiter, R. B. M. Schasfoort, R. Czajka, H. van Kempen, *Synth. Metals* **1992**, *51*, 397.

[96175]